Supporting Information

Engineering a surface functionalized Pt@SnS_2/$Ti_3C_2T_x$ MXene sensor with humidity tolerance and high sensitivity at room temperature for NH_3 detection

Kugalur Shanmugam Ranjith[a,], Sonam Sonwal[b], Ali Mohammadi[a], Ganji Seeta Rama Raju[a], Yun Suk Huh[b,*], Young-Kyu Han[a,*]*

[a]Department of Energy and Material Engineering, Dongguk University-Seoul, Seoul 04620, South Korea

[b]Department of Biological Engineering, Inha University, Incheon 22212, South Korea

[*]Corresponding authors: ranjuphy@gmail.com (K. S. Ranjith), yunsuk.huh@inha.ac.kr (Y. S. Huh), ykenergy@dongguk.edu (Y.-K. Han)

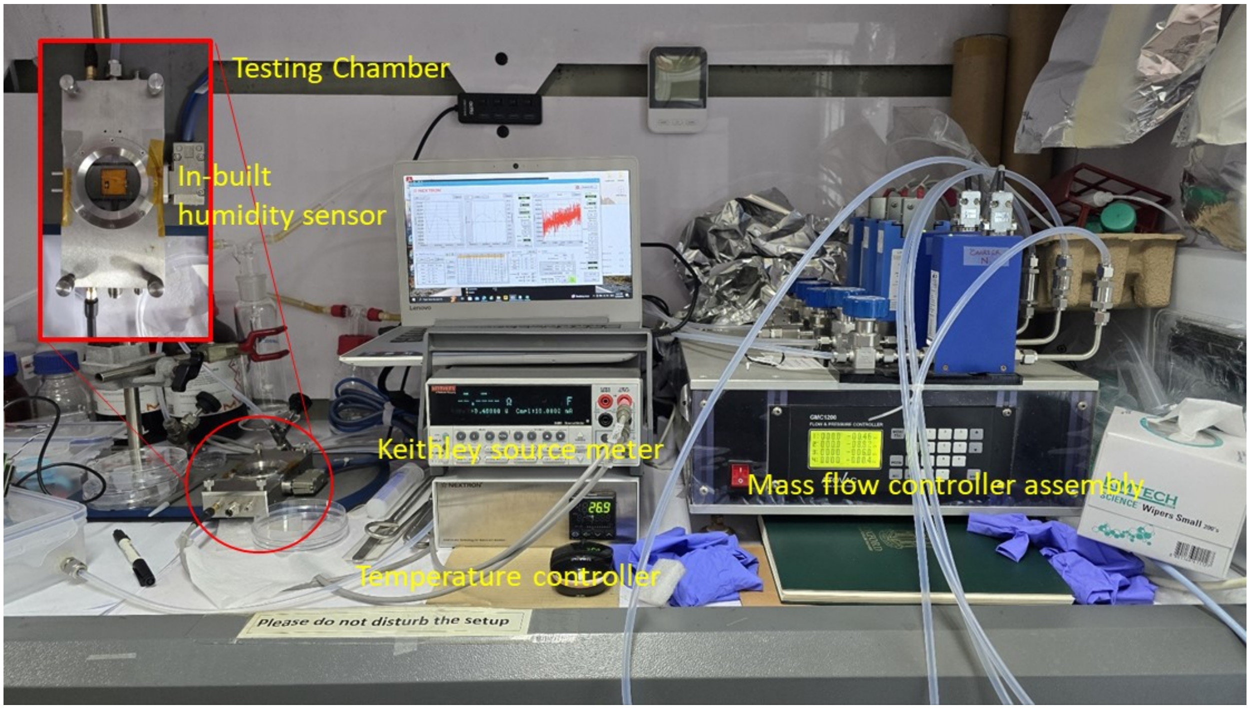

Fig. S1 The sensing setup assembly of Nextron microprobe system coupled with Keithley 2400 for the room temperature NH_3 sensing.

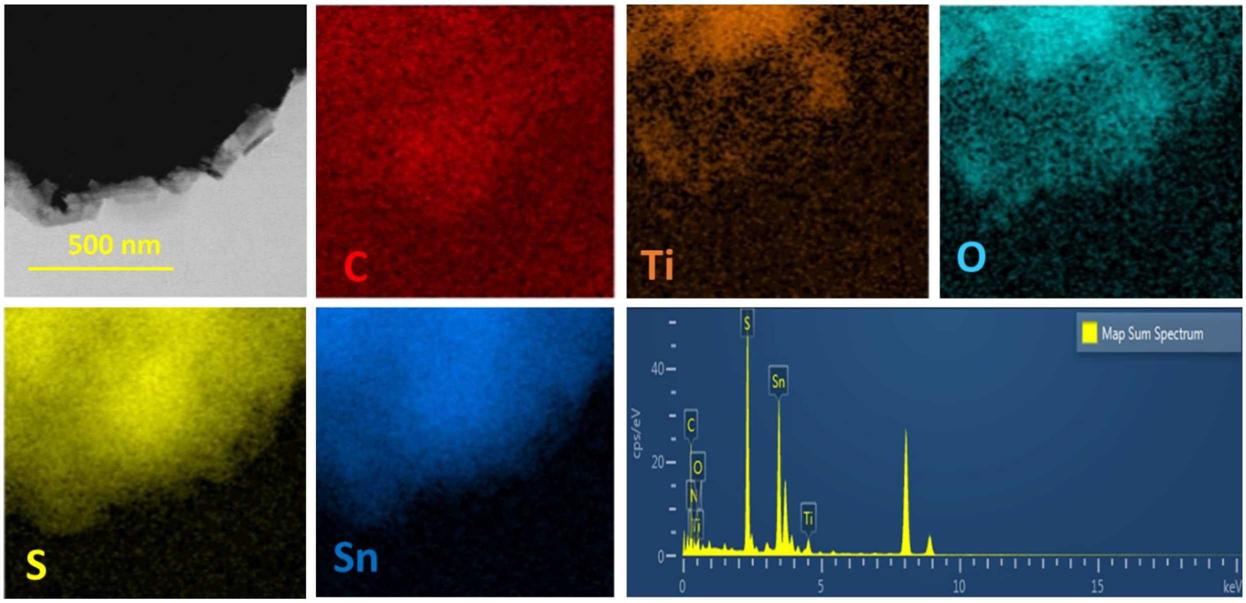

Fig. S2 The STEM and EDX mapping analysis of the SnS_2/MXene heterostructures.

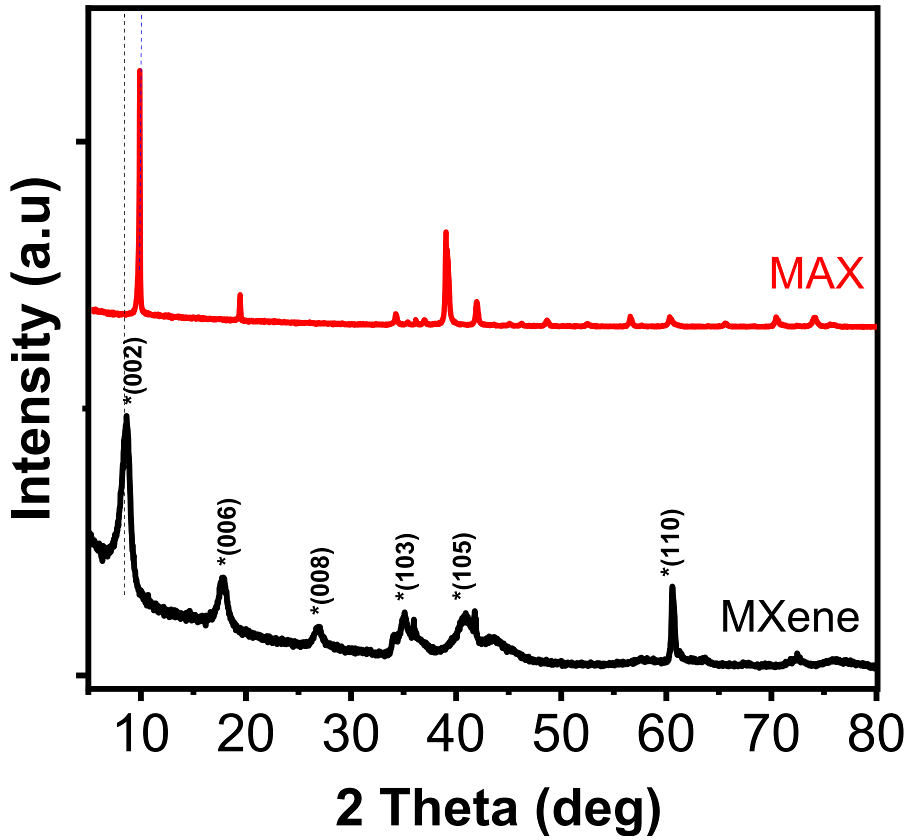

Fig. S3 XRD spectra of the MAX and MXene samples.

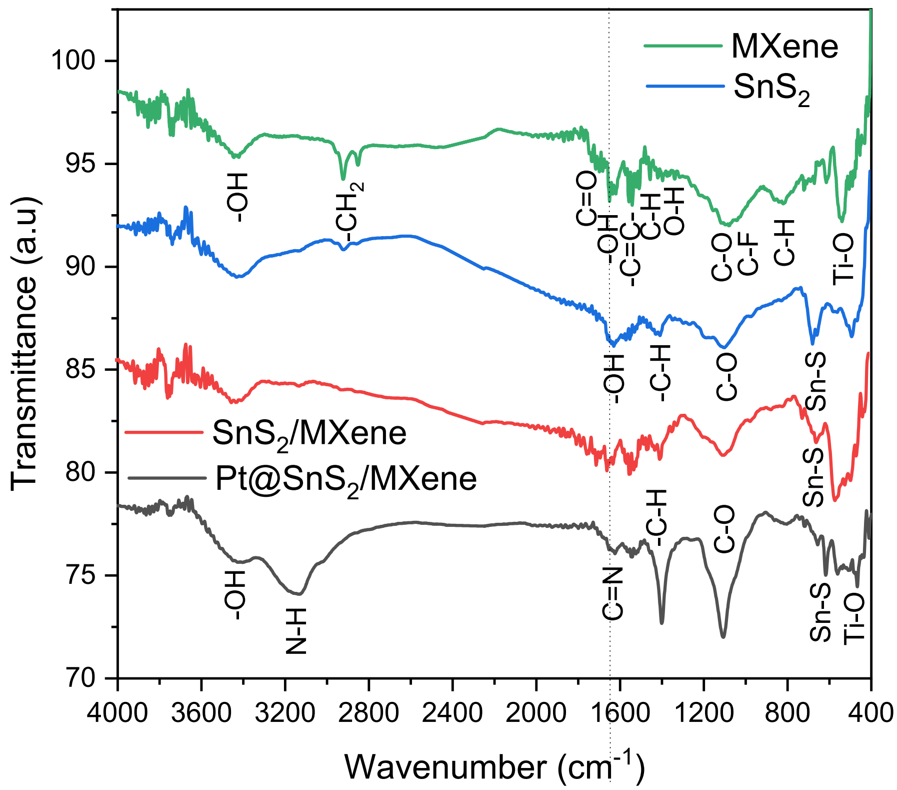

Fig. S4 The FTIR spectra of the MXene-based heterostructure samples.

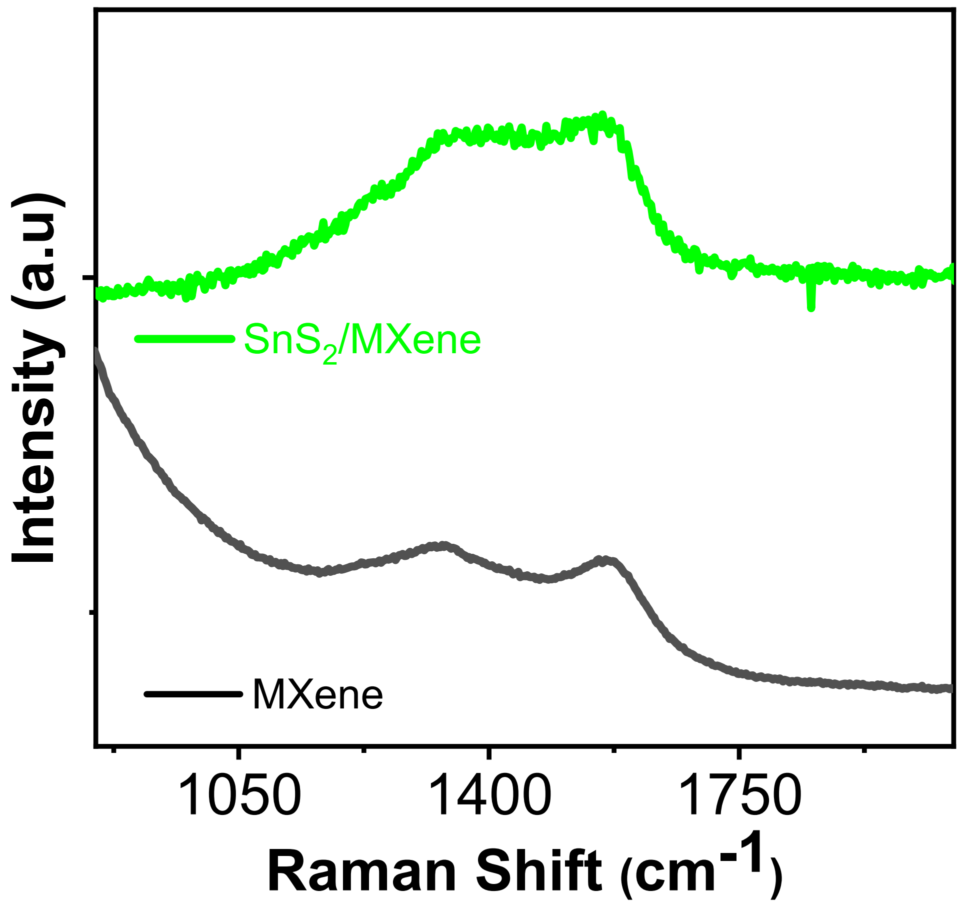

Fig. S5 The RAMAN spectra of the MXene and SnS_2/MXene samples.

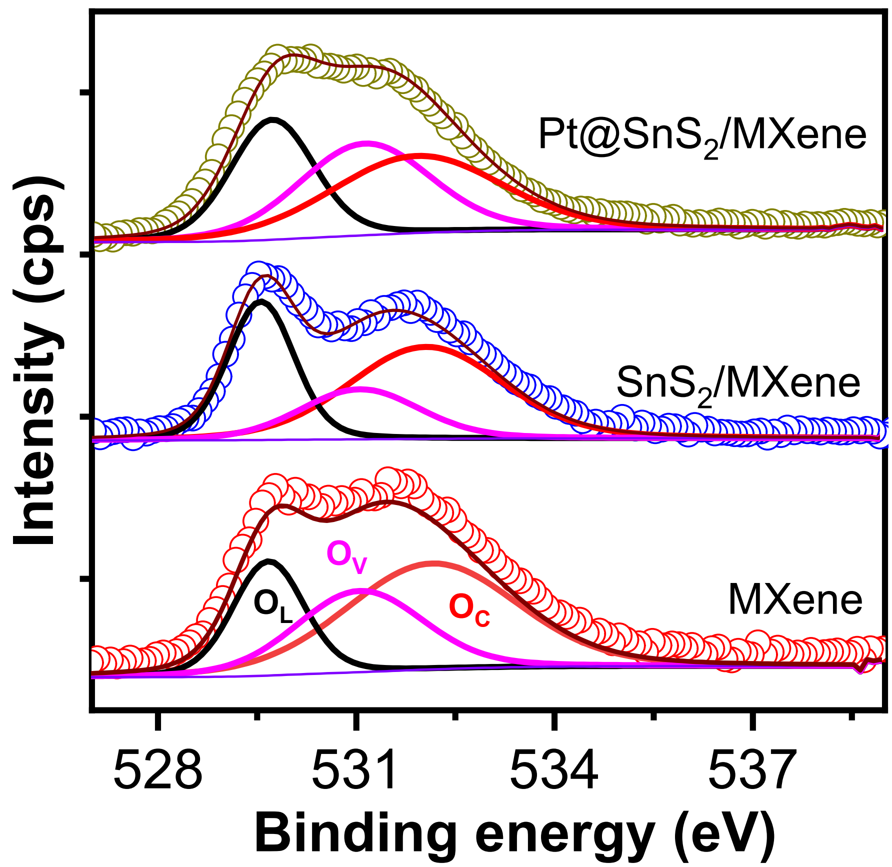

Fig. S6 The O 1s XPS spectra of the MXene-based heterostructures.

Table S1. Comparing the Oxygen related energy states in different heterostructure samples

Sample	Lattice oxygen (O_L) Binding energy (eV)	Area	Oxygen vacancy (O_V) Binding energy (eV)	Area	Chemisorbed oxygen (O_C) Binding energy (eV)	Area
MXene	529.9	10621.5	531.4	13411.3	532.6	23583.3
SnS_2/MXene	530.1	10345.6	531.6	6683.6	532.6	15903.5
Pt@SnS_2/MXene	530.3	14945.1	531.7	17962.8	532.5	19450.1

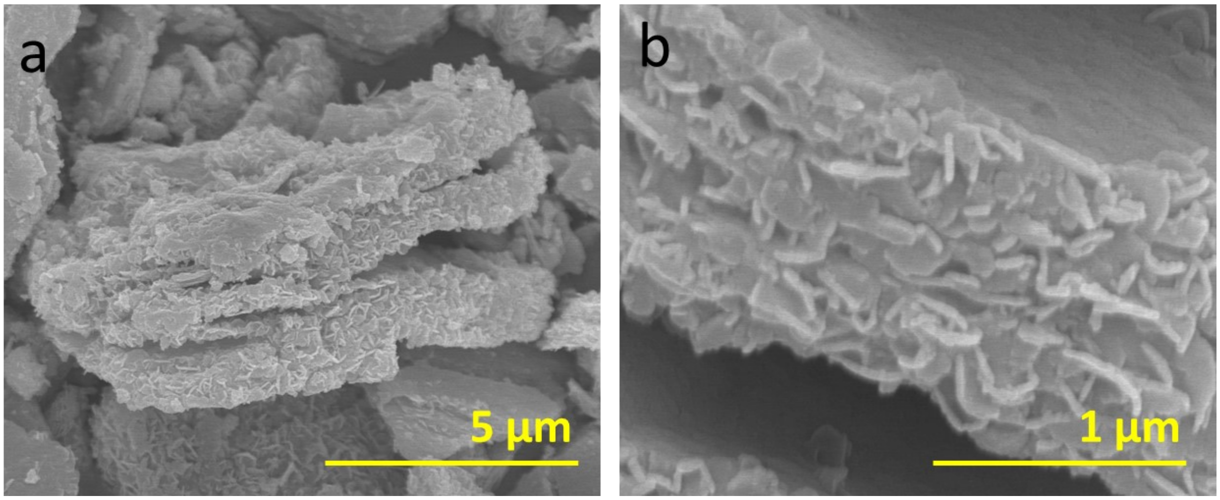

Fig. S7 The SEM images of the SAM-functionalized Pt@SnS_2/MXene heterostructures.

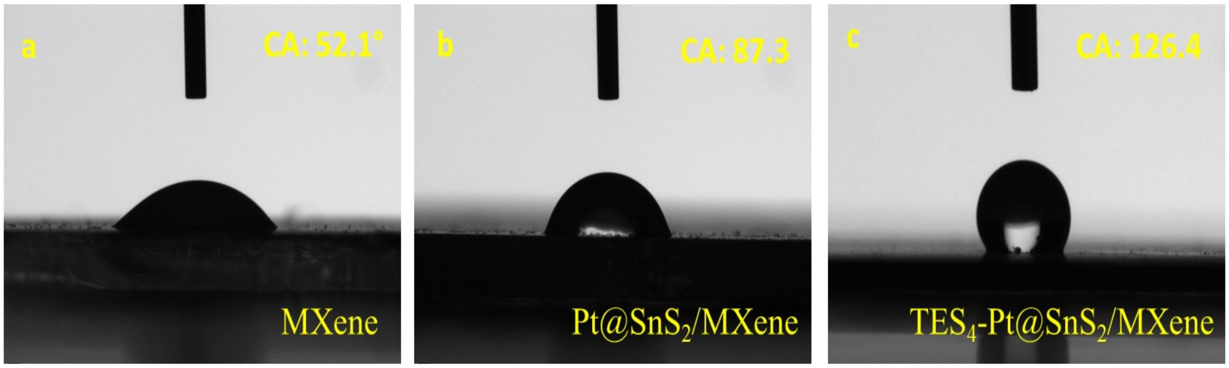

Fig. S8 The water contact angle of the (a) MXene, (b) Pt@SnS_2/MXene, and (c) TES_4-Pt@SnS_2/MXene heterostructures.

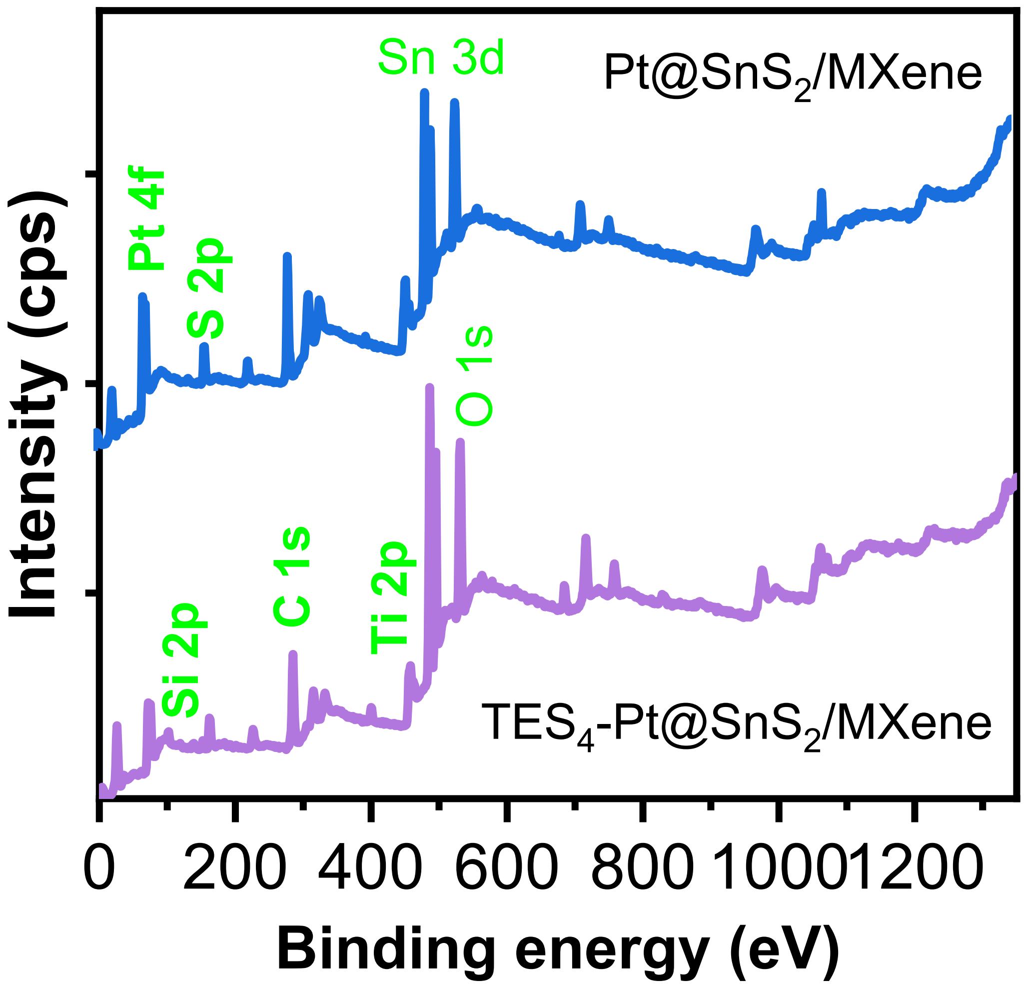

Fig. S9 The XPS survey spectrum of the Pt@SnS_2/MXene, and TES_4-Pt@SnS_2/MXene samples.

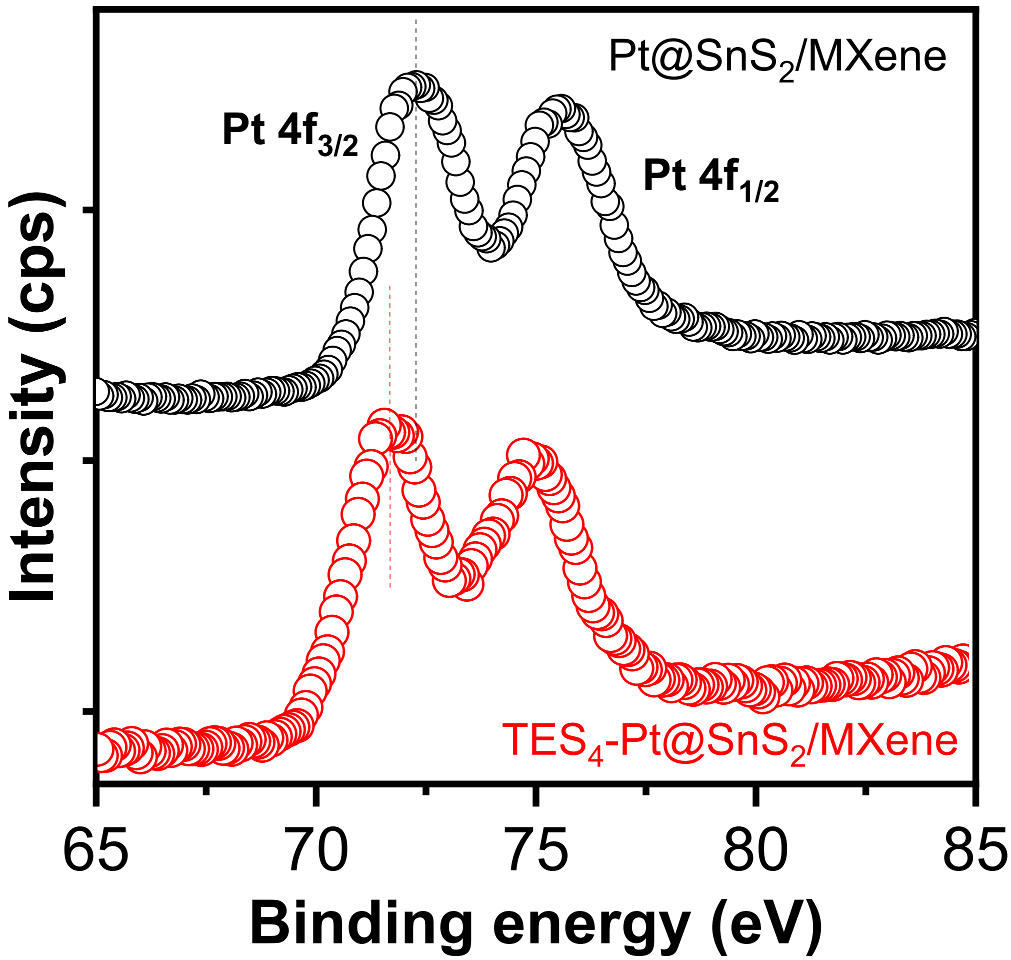

Fig. S10 The XPS Pt 4f spectra of the Pt@SnS_2/MXene, and TES_4-Pt@SnS_2/MXene samples.

Table S2. The Sensing response difference on the different SnS_2/MXene and different loading densities of Pt on SnS_2/MXene

Sample	Baseline resistance	Response
MXene	7.89E^{-3} Ohm	1.57
10wt%SnS_2/MXene	9.89E^{-4} Ohm	1.83
20wt%SnS_2/MXene	8.89E^{-6} Ohm	2.37
30wt%SnS_2/MXene	12.18E^{-6} Ohm	2.84
40wt%SnS_2/MXene	32.82E^{-6} Ohm	2.45
1wt%Pt@SnS_2/MXene	7.43E^{-6} Ohm	3.72
2wt%Pt@SnS_2/MXene	1.51E^{-6} Ohm	6.91
3wt%Pt@SnS_2/MXene	6.32E^{-6} Ohm	5.27
4wt%Pt@SnS_2/MXene	8.89E^{-5} Ohm	3.46

For Pt loading the 30wt%SnS_2/MXene is considered as optimum sample

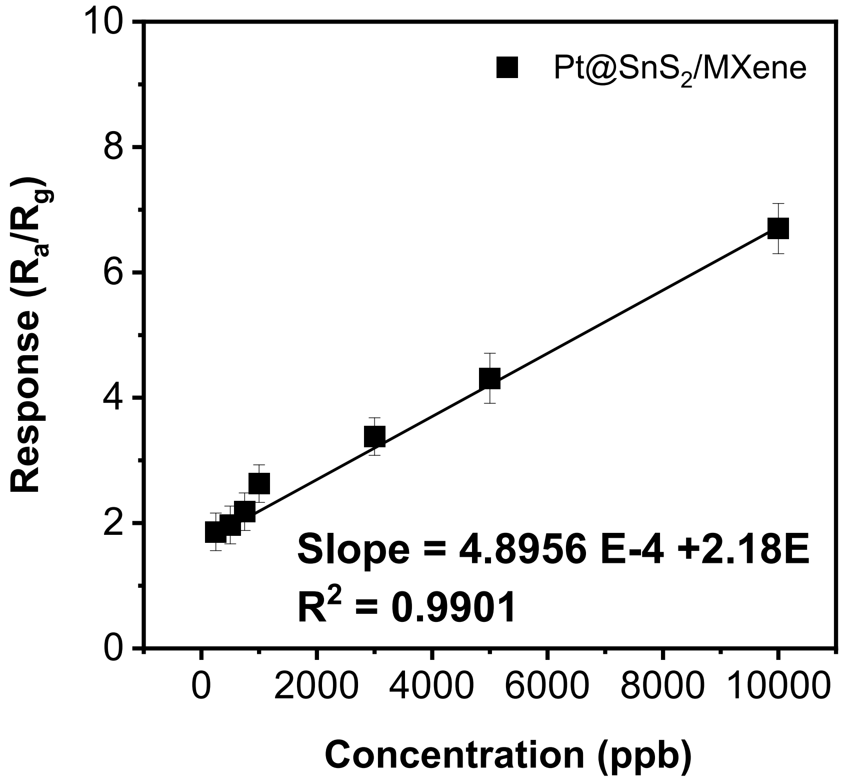

Fig. S11 The linear response to NH_3 with different concentrations on the Pt@SnS_2/MXene sensor.

Table S3. The Sensing result comparison of the MXene-based sensors reported in recent years.

Material	Temp	Analyte	Concentration	Response	LOD	Reference
$Ti_3C_2T_x$-F	RT	Ethanol	5 ppm	2.1[a]		[1]
$Ni_3(HITP)_2$/MXene	RT	NH_3	10 ppm	9.46	0.25 ppm	[2]
$Ni_3(HITP)_2$/MXene	RT	EtOH	10 ppm	28.8	0.005 ppm	[2]
$MoO_3/TiO_2/Ti_3C_2T_x$	RT	IPA	50 ppm	245%	--	[3]
MXene/TiO_2	RT	NH_3	10 ppm	3.1%	--	[4]
MXene/SnO_2	RT	NH_3	50 ppm	40%	--	[5]
$In_2O_3/Ti_3C_2T_x$	RT	Methanol	5 ppm	29.6%	--	[6]
$Ti_3C_2T_x$-ZnO	RT	NO_2	20 ppm	78.6%	--	[7]
V_2CT_x@MoS_2	RT	NH_3	1 ppm	8.71%	0.129 ppm	[8]
$Ti_3C_2T_x/TiO_2/MoS_2$	RT	NH_3	100 ppm	163.3%	0.5 ppm	[9]
$Ti_3C_2T_x$/graphene	RT	NH_3	100 ppm	7.2%	10 ppm	[10]
MXene/CuO	--	NH_3	100 ppm	24.8%	1 ppm	[11]
$Ti_3C_2T_x$/SnO	--	NH_3	10 ppm	67%	1 ppm	[12]
BiOCl/MXene	RT	NO_2	100 ppm	34.58[b]	0.03 ppm	[13]
$WO_3/Ti_3C_2T_x$	RT	NO_2	200 ppb	145%[a]	--	[14]
Pt SA-$Ti_3C_2T_x$	RT	TEA	2 ppm	175%[a]	--	[15]
Co-TCPP(Fe)/$Ti_3C_2T_x$-20	RT	NO	5 ppm	1.55[b]	0.2 ppm	[16]
MOF-MXene	RT	NH_3	10 ppm	13.37[a]	0.0128 ppm	[17]
Pt@SnS_2/MXene	RT	NH_3	10 ppm	6.72[b]	0.082 ppm	This work
TES_4-Pt@SnS_2/MXene	RT	NH_3	10 ppm	22.7[b]	0.023 ppm	This work

[a]Response (%) = $|(I_g - I_0)|/I_0 \times 100$ or $|(R_g - R_0)|/R_0 \times 100$, [b]Response = I_g/I_0

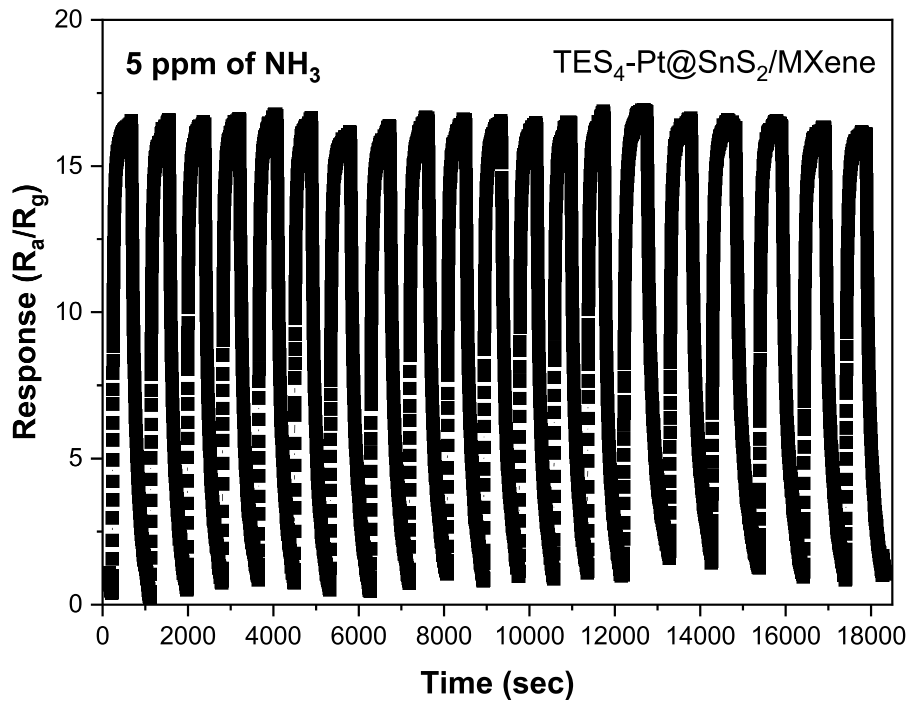

Fig. S12 Reproducibility of the TES_4-Pt@SnS_2/MXene sensor to 5 ppm of NH_3 at RT.

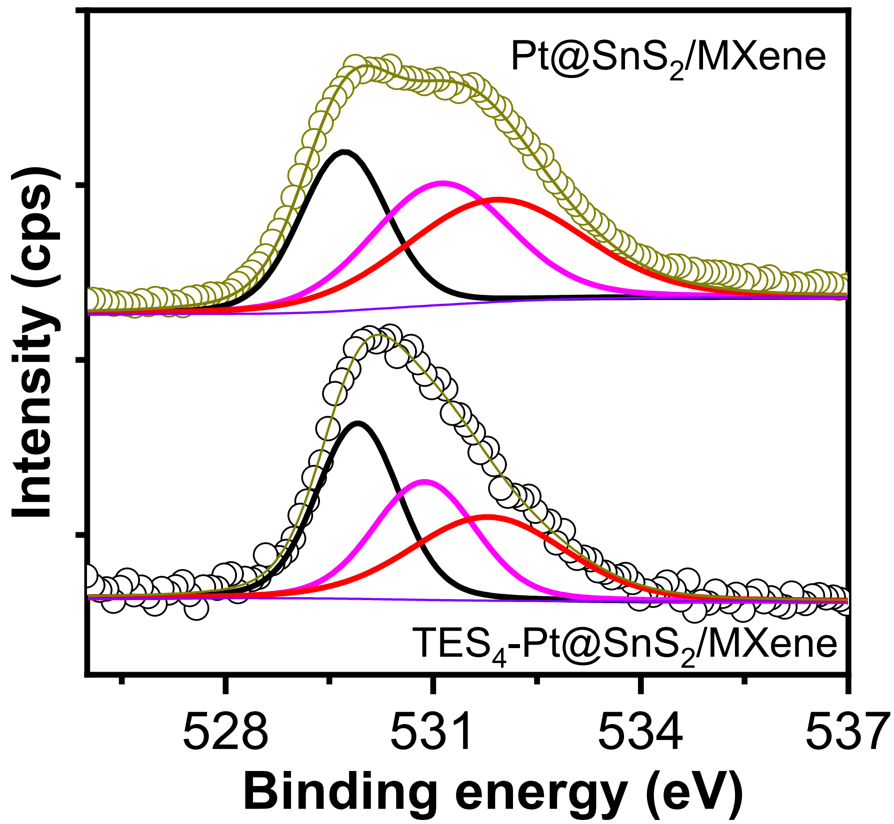

Fig. S13 The ex-situ XPS spectra of O 1s before and after the adsorption of NH_3 on the TES_4-Pt@SnS_2/MXene sample.

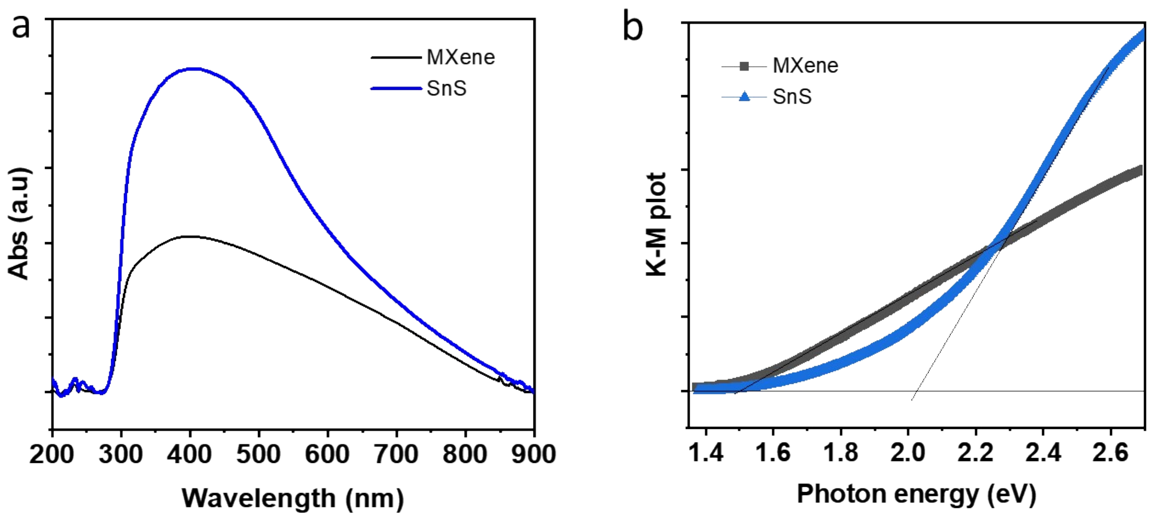

Fig. S14 (a) The UV vis absorption spectra and (b) K-M plot of the MXene and SnS_2 nanostructures.

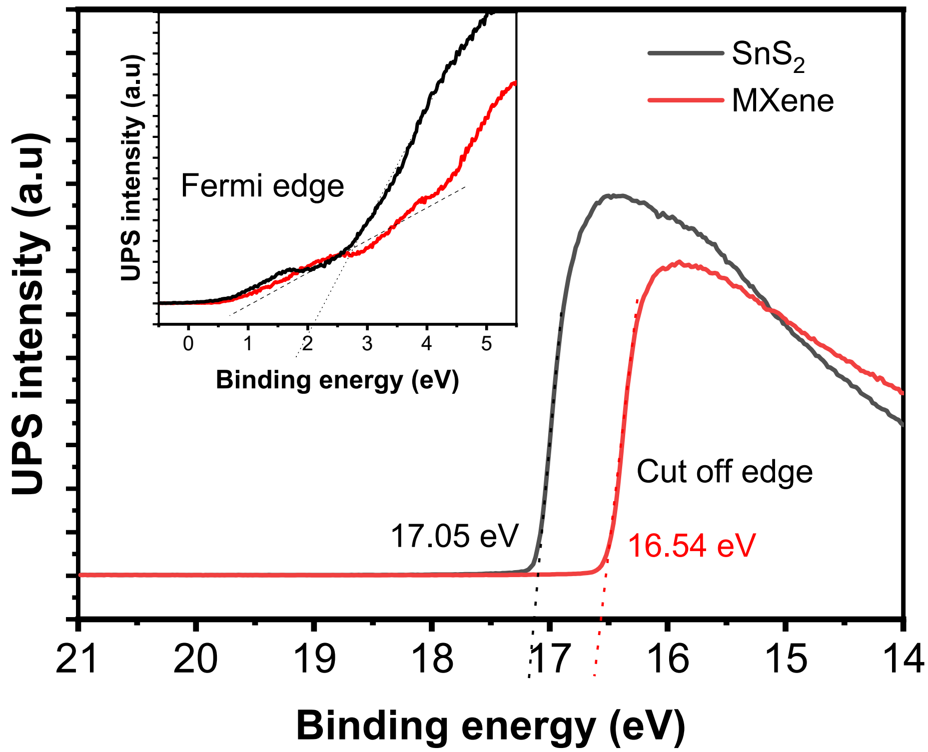

Fig. S15 The UPS spectra of the MXene and SnS_2 nanostructures.

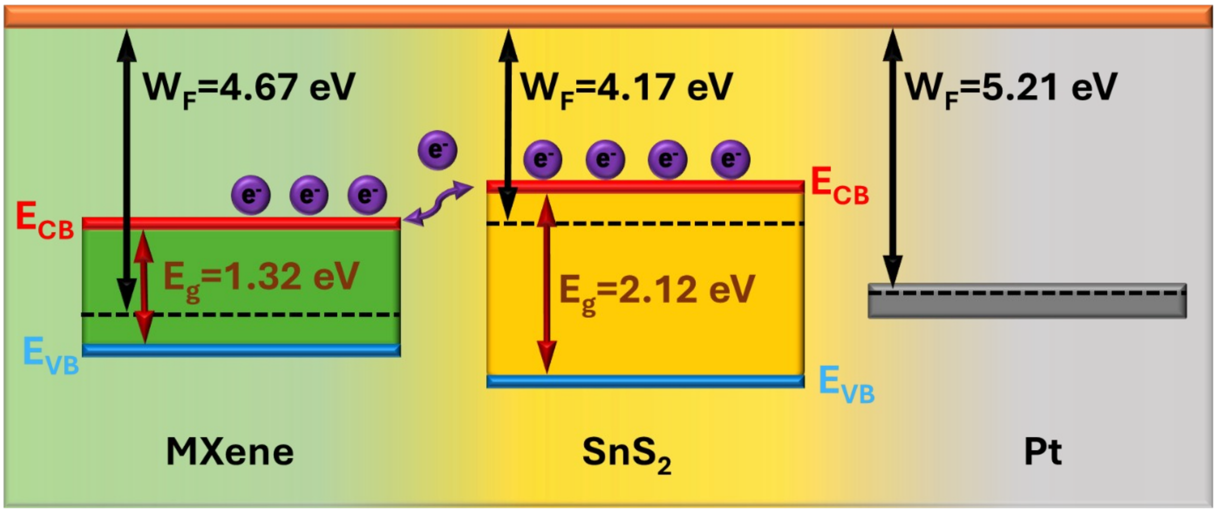

Fig. S16 Energy band structure of the MXene, SnS_2 with the Pt interface.

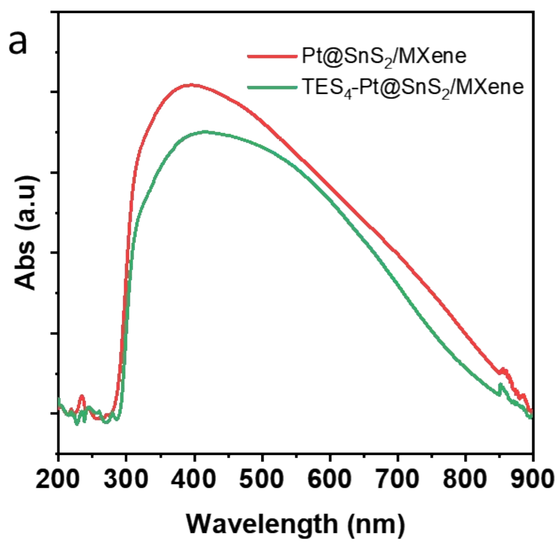

Fig. S17 (a) The UV vis absorption spectra and (b) K-M plot of the Pt@SnS_2/MXene and TES_4-Pt@SnS_2/MXene heterostructures.

References

1. W. Y. Chen, S. N. Lai, C. C. Yen, X. Jiang, D. Peroulis, L. A. Stanciu, Surface Functionalization of $Ti_3C_2T_x$ MXene with Highly Reliable Superhydrophobic Protection for Volatile Organic Compounds Sensing, *ACS Nano*, 2020, **14**, 11490–11501. https://doi.org/10.1021/acsnano.0c03896.
2. X. Wu, M. Niu, X. Tian, X. Peng, P. J. S. Buenconsej, X. Wu, Y. Wang, W. Ji, Y. Li, J. Qiao, J. Tao, M. Zhang, S. Xiao, H. Yuan, Solution-processable $Ni_3(HITP)_2$/MXene heterostructures for ppb-level gas detection, *J. Mater. Chem. A*, 2024, **12**, 17382-17394. https://doi.org/10.1039/D4TA02438A.
3. Y. Yao, Y. Han, M. Zhou, L. Xie, X. Zhao, Z. Wang, N. Barsan, Z. Zhu, $MoO_3/TiO_2/Ti_3C_2T_x$ nanocomposite based gas sensors for highly sensitive and selective isopropanol detection at room temperature, *J. Mater. Chem. A*, 2022, **10**, 8283-8292. https://doi.org/10.1039/D1TA11018G.
4. H. Tai, Z. Duan, Z. He, X. Li, J. Xu, B. Liu, Y. Jiang, Enhanced ammonia response of $Ti_3C_2T_x$ nanosheets supported by TiO_2 nanoparticles at room temperature, *Sensors and Actuators B: Chemical*, 2019, **298**, 126874, https://doi.org/10.1016/j.snb.2019.126874.
5. T. He, W. Liu, T. Lv, M. Ma, Z. Liu, A. Vasiliev, X. Li, MXene/SnO_2 heterojunction based chemical gas sensors, *Sensors and Actuators B: Chemical*, 2021, 329, 129275. *5Sens. Actuators, B*, 2021, **329**, 129275. https://doi.org/10.1016/j.snb.2020.129275.
6. M. Liu, Z. Wang, P. Song, Z. Yang, Q. Wang, In_2O_3 nanocubes/$Ti_3C_2T_x$ MXene composites for enhanced methanol gas sensing properties at room temperature, *Ceramics International*, 2021, **47**, 23028-23037, *Ceram. Int.*, 2021, **47**, 23028-23037.
7. M. Luo, X. Huang, D. Xiong, S. Cai, S. Li, Z. Jia, Z. Gao, Fast response/recovery and sub-ppm ammonia gas sensors based on a novel V_2CT_x@MoS_2 composite, *J. Mater. Chem. A*, 2024, **12**, 12225-12236. https://doi.org/10.1039/D4TA00842A.
8. X. Tian, L. Yao, X. Cui, R. Zhao, T. Chen, X. Xiao, Y. Wang, A two-dimensional $Ti_3C_2T_X$ MXene@TiO_2/MoS_2 heterostructure with excellent selectivity for the room temperature detection of ammonia, *J. Mater. Chem. A*, 2022, **10**, 5505-5519, https://doi.org/10.1039/D1TA10773A.
9. S. H. Lee, W. Eom, H. Shin, R. B. Ambade, J. H. Bang, H. W. Kim, T. H. Han, Room-

Temperature, Highly Durable $Ti_3C_2T_x$ MXene/Graphene Hybrid Fibers for NH_3 Gas Sensing, *ACS Appl. Mater. Interfaces*. 2020, **12**, 10434–10442, https://doi.org/10.1021/acsami.9b21765.

10. X. Wang, L. Gong, Z. Li, Y. Yin, D. Zhang, A room temperature ammonia gas sensor based on cerium oxide/MXene and self-powered by a freestanding-mode triboelectric nanogenerator and its multifunctional monitoring application, *J. Mater. Chem. A*, 2023, **11**, 7690-7701. https://doi.org/10.1039/D2TA07917H.
11. D. Wang, D. Zhang, Y. Yang, Q. Mi, J. Zhang, L. Yu, Multifunctional Latex/Polytetrafluoroethylene-Based Triboelectric Nanogenerator for Self-Powered Organ-like MXene/Metal–Organic Framework-Derived CuO Nanohybrid Ammonia Sensor, *ACS Nano* 2021, **15**, 2911–2919, https://doi.org/10.1021/acsnano.0c09015.
12. L. Yao, X. Tian, X. Cui, R. Zhao, M. Xiao, B. Wang, X. Xiao, Y. Wang, Two-dimensional $Ti_3C_2T_x$ MXene/SnO nanocomposites: Towards enhanced response and selective ammonia vapor sensor at room temperature, *Sensors and Actuators B: Chemical*, 2022, **358**, 131501, https://doi.org/10.1016/j.snb.2022.131501.
13. J. Fan, J. Gao, H. Lv, L. Jiang, F. Qin, Y. Fan, B. Sun, J. Wang, M. Ikram, K. Shi. Synthesis and characterization of an ultra-thin BiOCl/MXene heterostructure for the detection of NO_2 at room temperature with enhanced moisture resistance, *J. Mater. Chem. A*, 2022, **10**, 25714-25724. https://doi.org/10.1039/D2TA07924K.
14. S. Gasso, A. Mahajan, Development of Highly Sensitive and Humidity Independent Room Temeprature NO_2 Gas Sensor Using Two Dimensional $Ti_3C_2T_x$ Nanosheets and One Dimensional WO_3 Nanorods Nanocomposite, *ACS Sens.* 2022, **7**, 2454–2464, https://doi.org/10.1021/acssensors.2c01213.
15. B. Zong, Q. Xu, S. Mao, Single-Atom Pt-Functionalized $Ti_3C_2T_x$ Field-Effect Transistor for Volatile Organic Compound Gas Detection, ACS Sens. 2022, **7**, 1874−1882, https://doi.org/10.1021/acssensors.2c00475.
16. Y. Chang, M. Chen, Z. Fu, R. Lu, Y. Gao, F. Chen, H. Li, N. F. Rooij, Y. K. Lee, Y. Wang, G. Zhou, Building porphyrin-based MOFs on MXenes for ppb-level NO sensing, *J. Mater. Chem. A*, 2023, **11**, 6966-6977. https://doi.org/10.1039/D3TA00072A.
17. K. S. Ranjith, S. Sonwal, A. Mohammadi, G. S. R. Raju, M. H. Oh, Y. S. Huh, Y. K. Han, Imparting hydrophobicity to a MOF on layered MXene for the selective, rapid, and ppb

level humidity-independent , detection of NH_3 at room temperature, *J. Mater. Chem. A*, 2024, **Advance Article**, https://doi.org/10.1039/D4TA04656K.